Article

Not peer-reviewed version

Evaluation of *Limosilactobacillus reuteri* ATCC PTA 6127 Reveals Multilayered Protection Against Enteric Pathogens in a Canine Epithelial Model

Josh Walker [†], Akila Rekima [†], Andreea Cornelia Udrea, Katrine Bie Larsen, Adrian Schwarzenberg, Steffen Yde Bak, Niels Christensen, Svetlana Gerdes, Weiqing Zeng, Ashley Hibberd, Chong Shen [*]

Posted Date: 20 May 2026

doi: 10.20944/preprints202605.1341.v1

Keywords: *Limosilactobacillus reuteri*; canine epithelial cells; enteric pathogens; antimicrobial activity; epithelial wound healing

 doi:10.20944/preprints202605.1341.v1

Article

Evaluation of *Limosilactobacillus reuteri* ATCC PTA 6127 Reveals Multilayered Protection Against Enteric Pathogens in a Canine Epithelial Model

Josh Walker [1,†], Akila Rekima [2,†], Andreea Cornelia Udrea [2], Katrine Bie Larsen [2], Adrian Schwarzenberg [3], Steffen Yde Bak [3], Niels Christensen [3], Svetlana Gerdes [4], Weiqing Zeng [1], Ashley Hibberd [4] and Chong Shen [2,*]

[1] Direct-Fed Microbials Lab, R&D, Health & Biosciences, IFF, Nutrition Biosciences USA 1, LLC, 200 Powder Mill Road, Experimental Station - E361, Wilmington, 19803, DE, US

[2] Gut Immunology Lab, R&D, Health & Biosciences, IFF, Edwin Rahrs Vej 38, 8220 Brabrand, Denmark

[3] Enabling Technologies, R&D, Health & Biosciences, IFF, Edwin Rahrs Vej 38, 8220 Brabrand, Denmark

[4] R&D, Health & Biosciences, IFF, Madison, WI, US

* Correspondence: chong.shen@iff.com

† Contributed equally.

Abstract

Effective canine gastrointestinal health depends on suppression of enteric pathogens and maintenance of epithelial barrier integrity. *Limosilactobacillus reuteri* ATCC PTA 6127 (Lr6127) is a dog-derived probiotic, but evidence supporting its protective capacity remains limited. Here, we evaluated the antimicrobial and epithelial-supportive effects of Lr6127 using a canine epithelial cell model. Cell-free supernatant (CFS) from Lr6127 significantly inhibited the growth of canine-relevant pathogens, including *Escherichia coli* (52.0 ± 1.3%), *Clostridium perfringens* (54.0 ± 2.7%), and *Salmonella typhimurium* (48.6 ± 1.2%), compared with the medium control ($P < 0.0001$). Pathogen inhibition increased in a dose-dependent manner with increasing CFS concentrations. Untargeted metabolomic analysis revealed enrichment of multiple antimicrobial-associated metabolites, indicating multi-component pathogen suppression, with genomic analysis supporting the aromatic amino acid–derived metabolite findings. In addition, viable Lr6127 significantly reduced epithelial adhesion of all tested pathogens ($P < 0.01$). Beyond direct antimicrobial effects, Lr6127 CFS promoted epithelial wound healing at later time points, accompanied by coordinated modulation of proteins associated with cytoskeletal remodeling and barrier repair. Collectively, these findings suggest that Lr6127 is associated with pathogen suppression, reduced adhesion, and epithelial wound repair mechanisms.

Keywords: *Limosilactobacillus reuteri*; canine epithelial cells; enteric pathogens; antimicrobial activity; epithelial wound healing

1. Introduction

The canine gastrointestinal tract plays a central role in nutrient absorption, immune surveillance, and protection against enteric pathogens. Disruption of this ecosystem—through dietary transitions, stress, antibiotic exposure, or infection—commonly leads to gastrointestinal disease manifested as acute or chronic diarrhea, mucosal inflammation, and compromised barrier function [1]. Enteric bacterial pathogens are a major contributor to these disorders in dogs, both in clinical practice and under conditions of environmental or dietary challenge [1].

Among these pathogens, *Escherichia coli*, *Clostridium perfringens*, and *Salmonella enterica* represent clinically and mechanistically distinct threats to canine gut health, yet converge in their capacity to disrupt epithelial function and compromise intestinal barrier integrity [1–3]. Canine associated pathogenic *E. coli* comprise multiple toxin-producing pathotypes rather than a single virulence

 doi:10.20944/preprints202605.1341.v1

mechanism [4]. *Enterotoxigenic E. coli* strains producing heat-stable enterotoxins STa and STb disrupt epithelial ion transport through cyclic nucleotide- and calcium-dependent signaling pathways, resulting in secretory diarrhea [5], a disease phenotype reported in dogs with enteric E. coli infection [4]. Strains expressing heat-labile enterotoxin (LT) further perturb epithelial ion transport via cAMP-mediated mechanisms, contributing to fluid loss and epithelial dysfunction [5]. In contrast, Shiga toxin-producing E. coli expressing STx variants exert direct cytotoxic effects on epithelial cells, leading to epithelial barrier damage and inflammatory responses rather than purely secretory diarrhea [3].

Clostridium perfringens further contributes to canine enteric disease, with toxin type A strains predominating in diarrheic dogs [1,6]. These strains produce α-toxin and *C. perfringens* enterotoxin, which disrupt epithelial membranes, impair tight junction integrity, and promote mucosal inflammation [6]. The presence of additional pore-forming toxins in type A strains has strengthened the causal link between toxin-mediated epithelial injury and severe canine disease phenotypes, including acute hemorrhagic diarrhea syndrome [7].

Salmonella enterica, particularly serovar *Typhimurium*, represents a mechanistically distinct challenge in the canine gut. Following ingestion, *S. Typhimurium* invades intestinal epithelial cells and activates pro-inflammatory signaling cascades that drive inflammatory enterocolitis and epithelial damage [2]. Although infection in dogs is often self-limiting, disease severity increases under conditions of stress, dietary perturbation, or immune compromise, and asymptomatic carriage poses ongoing risks to both canine and public health [2]. Collectively, these pathogens illustrate complementary but clinically relevant modes of epithelial disruption in dogs—ranging from toxin-mediated secretory diarrhea and cytotoxic injury to invasive inflammatory damage—underscoring the need for interventions that target both pathogen activity and epithelial defense.

Probiotics are increasingly explored for their potential to help maintain host defenses.. Beyond direct antimicrobial effects, probiotics have been reported to reduce pathogen colonization through competitive exclusion at epithelial surfaces [8], secrete bioactive metabolites that suppress pathogenic growth and virulence [9], and are associated with improved epithelial barrier function by promoting cellular repair and cytoskeletal reorganization [8]. Among probiotic species, *Limosilactobacillus reuteri* has attracted particular interest due to its capacity to produce organic acids and indole-derived metabolites with antimicrobial and host-modulatory properties [8], as well as its documented influence on epithelial signaling pathways involved in migration and wound repair [8]. Notably, canine-derived *L. reuteri* strains have demonstrated bacteriostatic activity, gastrointestinal resilience, and favorable safety profiles, supporting their relevance for dog-specific applications rather than extrapolation from human or livestock models [10].

In the present study, we investigated *Limosilactobacillus reuteri* ATCC PTA 6127 (Lr6127), a well-characterized probiotic strain which was isolated from a dog, for its potential to support canine gut health through complementary antimicrobial and host-directed mechanisms. We hypothesized that Lr6127 is associated with reductions in pathogen growth and adhesion, and may be linked to enhanced epithelial wound closure.. Using a canine epithelial cell model, we examined pathogen growth inhibition and adhesion exclusion, characterized antimicrobial metabolites present in Lr6127 cell-free supernatant, assessed epithelial wound healing, and quantified changes in wound-healing-associated protein abundance. Together, this integrated in vitro approach provides contextual insight into responses associated with Lr6127 reinforcing epithelial barrier resilience and mitigating pathogen-associated risk in the canine gut.

2. Materials and Methods

2.1. Reagents and Materials

All cell culture media, equipment and reagents were purchased from Thermo Fisher Scientific (Roskilde, Denmark) unless otherwise stated.

 doi:10.20944/preprints202605.1341.v1

2.2. Bacterial Strains, Culture Conditions, of Cell-Free Supernatant Preparation and Cell Line

The probiotic strain *Limosilactobacillus reuteri* (ATCC PTA-6127; PureStrong™, Lr6127) was characterized by and licensed from BioGaia AB (Stockholm, Sweden). *Escherichia coli, Clostridium perfringens*, and *Salmonella typhimurium* were obtained from the Danisco Global Culture Collection (DGCC; Niebüll, Germany). Species identification and genetic characterization are summarized in Supplementary Table S1.

Lr6127 was cultured with de Man–Rogosa–Sharpe (MRS) agar and broth at 37°C. *C. perfringens* pathogen strains were grown on Brain–Heart Infusion (BHI) agar and in Reinforced Clostridial Medium + 0.1% Sodium Resazurin (RCM) broth, at 37 °C under anaerobic conditions using Oxoid AnaeroGen sachets. *E. coli* and *S. typhimurium* were cultured on Tryptic Soy Agar (TSA) and Broth (TSB) at 37 °C under aerobic conditions.

Cell-free supernatant (CFS) was prepared from Lr6127. Lr6127 colonies were grown from glycerol freezer stocks by streaking on agar followed by overnight incubation. Individual colonies were collected and resuspended by pipetting in MRS medium in a 2 mL microtube, allowing large particulates to settle. The upper fraction of the suspension was transferred to a new container, and optical density was measured at 600 nm (OD600). All optical density measurements were done using a Synergy MX microplate reader (BioTek Instruments, Inc., Highland Park, VT, USA). The volume of this suspension equivalent to 50uL at OD600 of 1, was calculated using the following formula:

$$x \text{ volume of suspension required} = 50\ \mu L / (ODx - ODy)$$

where:

ODx = OD600 of cell suspension

ODy = OD600 of culture media alone

This approximation assumes that OD decreases linearly with dilution. Only OD_x values below 1.5 were accepted; cultures exceeding this threshold were diluted with additional fresh medium and remeasured. The calculated suspension volume was used to inoculate 25 mL of the appropriate broth in a 125 mL flat-bottom flask. Cultures were incubated for 6 h, after which OD_{600} was measured again. The culture volume equivalent to 10uL of culture at OD_{600} of 1 was calculated using the same approach, by substituting 50 µL with 10 µL in the formula. This volume was used to inoculate 50 mL of broth in a 250 mL flat-bottom flask, which was incubated with gentle shaking for 18 h. The culture was then centrifuged at 5000 × g for 5 min, and the resulting supernatant was sterilized by vacuum filtration through a 0.2 µm filter (Thermo Scientific Nalgene, 500 mL, aPES membrane, 75 mm diameter, #566-0020) to generate CFS. CFS preparations were stored at −20 °C until use.

The canine proximal epithelial cell line MCA-B1 (DSMZ; Braunschweig,

Germany; ACC 828) was propagated in DMEM/F12 medium supplemented with 10% heat-inactivated fetal bovine serum (FBS) and 1% penicillin–streptomycin (100 U/mL penicillin, 100 µg/mL streptomycin). CFS was added to cell cultures at a maximum of 5% (v/v) and cultured overnight at 37 °C with 5% CO_2 environment. Prior testing confirmed that this did not alter the final medium pH, which remained between 7.0 and 7.2. Optical density values were correlated with colony-forming units (CFU) by serial dilution and plate counts (OD_{600} = 1.0 corresponding to approximately 1×10^9 CFU/mL). All experiments used CFS at a working concentration equivalent to secretions from 1×10^7 CFU/mL

2.3. Pathogen Inhibition Assay

CFS from Lr6127 was tested for inhibitory activity against porcine *E. coli*, *C. perfringens*, and *S. typhimurium* isolates (Supplementary Table S1). Colonies of pathogenic bacteria were resuspended in duplicate in 200 µL of the appropriate broth in 96-well microplates (Corning #3474) and incubated at 37 °C with shaking for 4 h. These preliminary cultures were used to inoculate duplicate assay plates containing the pathogen's growth medium supplemented with Lr6127 CFS. Wells containing no CFS served as medium controls (0% CFS). For *E. coli* and *Salmonella* assays, wells contained 20% (v/v) CFS and 1% (v/v) inoculum, whereas *C. perfringens* assays used 20% (v/v) CFS and 4% (v/v) inoculum

 doi:10.20944/preprints202605.1341.v1

(Figure 1A). The final volume per well was 200 µL. For the dose-response assay (Figure 1B), assays were set up with CFS volumes of 0%, 5%, 10%, 15%, and 20% (corresponding to 0, 10, 20, 30, 40uL). For conditions under 20% CFS, the remaining volume was replaced with MRS, so that each condition had a total of 20% of MRS and/or CFS (spent MRS). All plates were incubated at 37 °C for 16 h with shaking at 200 rpm, after which OD_{600} was measured, and the percentage growth inhibition was calculated using the following equation:

$$\% \text{ inhibition} = [(1 - (ODa - OD0) / (ODb - OD0))] \times 100$$

where:

ODa = OD600 of media containing pathogen inoculum and probiotic CFS (challenge well)

OD0 = OD600 of media without inoculum or probiotic CFS (negative control)

ODb = OD600 of media containing pathogen inoculum but without probiotic CFS (unchallenged / medium control)

Experiments were performed three times with three replicates per experiment.

As a quality control step, absorbance measurements from isolates exhibiting insufficient growth—defined as an $OD_{600} < 0.5$ in the medium control—were excluded from further analysis. Outliers were identified using the interquartile range (IQR) method, with values exceeding $Q3 + 1.5 \times IQR$ or below $Q1 - 1.5 \times IQR$ removed from the dataset. Following QC filtering, mean percentage inhibition values were calculated for 8 *Escherichia coli*, 9 *Clostridium perfringens*, and 5 *Salmonella typhimurium* isolates.

(**A**)

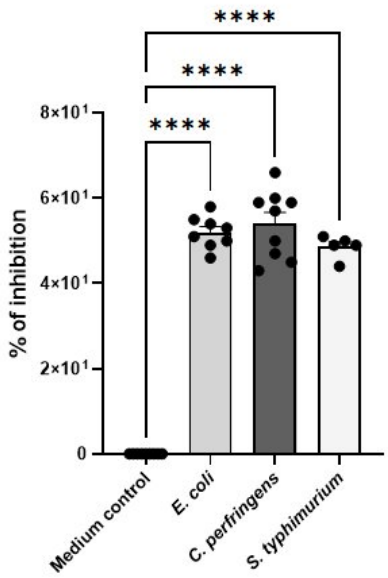

(**B**)

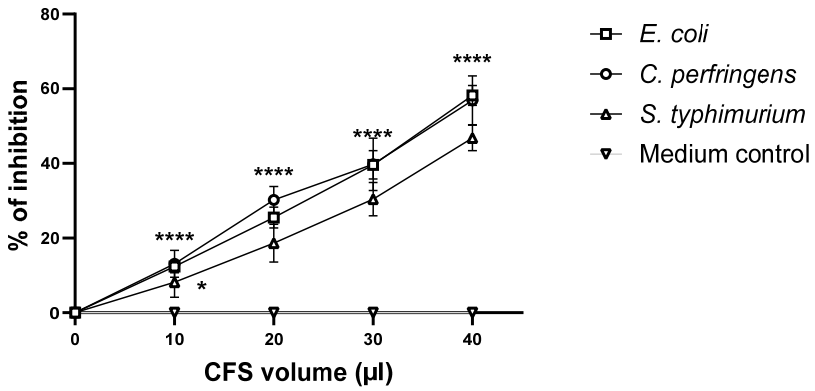

 doi:10.20944/preprints202605.1341.v1

Figure 1. Effect of *Limosilactobacillus reuteri* 6127 (Lr6127) cell-free supernatant (CFS) and medium control on the growth of *Escherichia coli, Clostridium perfringens,* and *Salmonella typhimurium* isolates. (A) Growth inhibition after 16 h of incubation, expressed as percentage inhibition normalized to the medium-only control. (B) Growth inhibition increased in a dose-dependent manner with increasing volumes of Lr6127 CFS added to the culture. Values are presented as means ± standard error (SE). Experiments were performed three times with three technical replicates per experiment. Pairwise comparisons were performed relative to the medium control. In panel B, data points at 10–40 µL CFS were compared to the 0 µL control. All comparisons yielded $P < 0.0001$, except for *S. typhimurium* at 10 µL CFS ($P < 0.05$). * $P < 0.05$; **** $P < 0.0001$.

2.4. Untargeted Metabolomics of CFS Supernatants

Lr6127 cell-free supernatant (CFS) was generated as previously described, with MRS medium cultured under identical conditions serving as the medium control. Samples were randomized and diluted in a 1:1 ratio with H_2O: MeOH using an Opentrons Flex automated liquid-handling system. A pooled quality control (QC) sample was created by combining aliquots from all experimental samples and was analyzed after every ten injections.

Metabolomic analysis was conducted using a 1290 Infinity III UHPLC system (Agilent Technologies, Glostrup, Denmark) coupled to a timsTOF Flex MALDI 2 mass spectrometer (Bruker, Roskilde, Denmark). Chromatographic separation was performed on an Acquity UPLC HSS T3 column employing a water–acetonitrile gradient containing 0.1% formic acid. Samples were injected at a volume of 5 µL with a flow rate of 0.25 mL/min. Data acquisition was carried out in both positive and negative ionization modes using a VIP HESI source, with MS/MS spectra collected via parallel accumulation–serial fragmentation (PASEF) over an m/z range of 100–1350. Internal mass calibration was achieved using sodium formate and an Agilent low-concentration tuning mix.

Raw data were processed in MetaboScape (version 2026) using the T-Rex 4D feature detection algorithm, integrating m/z, retention time, ion mobility, and intensity information. Metabolite annotation was based on in-house MS^2 libraries and public databases, including GNPS, LipidBlast, Bruker NIST HRMS, MetaboBase Personal Library 3.0, and HMDB.

2.5. Phylogenetic Analysis of Lr6127

A high-quality bacterial genome of Lr6127 was assembled using Autocycler v0.2.1 [11] by integrating long reads generated with the MinION platform (Oxford Nanopore Technologies, Oxford, UK) and short reads sequenced on the NextSeq1000 sytstem (Illumina, San Diego, USA). The genome consisted of 2,222,416 bp in 2 contigs with a G+C content of 38.7%. Taxonomy was verified by whole genome average nucleotide identity (ANI), which showed 96.5% nucleotide identity to the type strain DSM 20016, consistent with assignment to the species *L. reuteri.*

2.6. Lr6127 Adhesion and Pathogen Exclusion Assays

Lr6127 adhesion: The adhesion assay was performed as previously described by Rasmussen et al. [12]. In brief, MCA-B1 cells were seeded in 96-well plates at a density of 2×10^4 cells/well in a total volume of 0.2 mL and grown for two days until 100% confluency. Lr6127 grew in MRS at 37 °C under anaerobic conditions for 24 h, the OD measured at 600 nm and the concentration adjusted to an OD of 1.00. A 30 µl sample of Lr6127was then added directly onto the MCA-B1 cells in each well in 96 well plates and the cells co-cultured for 30 min at 37 °C (CFU_{loaded}). The cell monolayer was then washed five times with PBS and the cells lysed with cold 0.1% Triton X-100 solution. The lysates were then serially diluted (10-fold) in PBS and plated onto MRS agar for the enumeration of adherent bacteria ($CFU_{adhered}$). Plates were cultured at 37 °C for 24 h before colony counting. For the identification of bacteria loaded (CFU_{loaded}), the bacterial suspension prior to its addition to the MCA-B1 cells was also serially diluted in parallel and plated onto MRS plates. The percentage adhesion of Lr6127 to the MCA-B1 cells was calculated according to the following formula:

$$\text{Cell adhesion (\%)} = [(CFU_{adhered})/(CFU_{loaded})] \times 100$$

 doi:10.20944/preprints202605.1341.v1

The data are means from 3 experiments with 5 replicates per experiment.

Pathogen exclusion: the exclusion assay is to determine the capacity of Lr6127 to exclude *E. coli, C. perfringens*, and *S. typhimurium* from adhering to MCA-B1 cells when applied to cells before their application. The assay was performed in a similar manner to that described by Rasmussen et al. [12] but adapted for study in canine cells. In brief, in the exclusion assay, MCA-B1 cells were seeded into plates at a density of $2*10^4$ cells/well and grown to 100% confluency. Fresh cultures of Lr6127 were prepared, their OD measured and adjusted to an OD of 1.00, and the bacteria loaded directly onto MCA-B1 cells as described for the adhesion assay. The 8 test *E. coli, 9 C. perfringens*, and 5 *S. typhimurium* isolates (as listed in Supplementary Table S1.) were grown in culture media and the OD of each culture adjusted to an OD of 1.00 as for the Lr6127 cultures. A 300 µL sample of each resulting pathogen culture was then centrifuged and then, the pellet resuspended in 30 µL of culture medium and the resulting suspension added directly to the Lr6127 MCA-B1 cell coculture without a washing step. The cells were then incubated at 37 °C for 30 minutes. After incubation, the MCA-B1 cells were washed (five times with PBS) and lysed with 0.1% Triton-X solution, as before. The lysates were serially diluted (10-fold) and loaded onto either LAMVAB agar plates (MRS agar with 20 mg/L vancomycin, for the enumeration of Lr6127, CFU_{Lr6127}) and MacConkey plates (for the enumeration of *E. coli*, CFU_{EC}). Plates were cultured as for the adhesion assay, the CFU counted ($CFU_{adhered}$) and the percentage of adhered cells calculated, as in the cell adhesion assay.

The reduction in the percentage adhesion (here termed 'exclusion') in the Lr6127-treated groups compared to the response in the medium control (MCA-B1 cells with *E. coli* but without Lr6127) was calculated according to the following equation:

the percentage *E. coli* adhered was calculated according to the following equation:

$$\%\ E.\ coli_{\ adhered}\ (\%EC_{\ adhered}) = (CFU_{EC\ adhered}/\ (CFU_{EC\ loaded})\ ´\ 100$$

$$\text{Exclusion}\ (\%) = [1 - (\%EC_{\ adhered,\ with\ Lr6127}/\ \%EC_{\ adhered,\ without\ Lr6127}]\ ´\ 100$$

Lr6127 exclusion *C. perfringens* or *S. typhimurium* assay were performed in a similar procedure, except lysate was placed on CP ChromoSelect (Merck, Søborg, Denmark) or Chromaga Salmonella for numeration respectively. Experiments were performed three times with night replicates in total.

2.7. Wound-Healing Assay

A wound-healing assay was performed using a culture-insert 2 well in a µ-Dish 35 mm (Ibidi, Gräfelfing, Germany). Briefly, MCA-B1 epithelial cells were seeded at a density of 6×10^5 cell/mL cells outside the insert area allowing cell attachment and growth around the insert overnight at 37 °C in an atmosphere of 5 % CO2 to obtain confluent cell layer. The insert was then gently removed with sterile tweezers to create a gap. The cell layer is washed with culture media to remove cell debris and non-attached cells. The cells were then incubated with fresh media supplemented with CFS from Lr6127 (equivalent to 10^7/CFU/mL) or with MRS media (Medium control).

Wound closure was monitored using an inverted microscope (Eclipse Ts2R, Nikon, Ramcon, Aarhus, Denmark) with a 4x magnification objective, and images were acquired immediately after insert removal on day 0 and wound area was measured in the following 10 days and quantified manually using the Nikon Imaging Software (NIS-Elements, Nikon, The Netherlands) and expressed area under curve according to the following: The wound area value was first been converted into Logarithmic scale (in-Scale). Individual data was then normalized using the mean value of the control group as center. The area under curve from day 1 to day 10 was expressed by the sum up respectively and used for comparison between 2 groups. Experiment was performed with three replicates in each treatment group.

2.8. Proteomic Profiling of MCA-B1 Cells Following Lr6127 CFS Exposure

MCA-B1 cells were prepared as previously described and grown to full confluence. Fresh culture medium was applied, followed by the addition of Lr6127 cell-free supernatant (CFS) at a

 doi:10.20944/preprints202605.1341.v1

concentration corresponding to 1×10^7 CFU/mL Plates were maintained overnight at 37 °C in a humidified atmosphere containing 5% CO_2. Control samples received DMEM supplemented with MRS only. Eight biological replicates were included per treatment.

Cells were rinsed with PBS and lysed using a solution containing 5% SDS, 100 mM triethylammonium bicarbonate, and protease inhibitor cocktail (Roche Diagnostics, Merck Life Science, Copenhagen, Denmark). Proteomic analysis was conducted in accordance with the protocol described by Kadekar et al. [13]. Peptide separation and analysis were performed using a Vanquish Neo UHPLC system coupled to a Q Exactive HF mass spectrometer. A trap-and-elute configuration was employed using a NanoViper trap column and a Waters nanoEase M/Z Peptide BEH C18 analytical column, with a 70-minute gradient at a flow rate of 2000 nL/min. Data-dependent acquisition with HCD fragmentation was applied.

Raw mass spectrometry data were processed using Proteome Discoverer version 3.0 and searched against the UniProt *Canis familiaris* protein database using the Mascot search engine.

2.9. Statistical Analysis

For assays other than protein expression, group differences were assessed using the Kruskal–Wallis H test (one-way analysis of variance on ranks). For comparisons between two groups, the Mann–Whitney U test was used. Results were considered significant at $P < 0.05$. Protein expression data were subjected to multivariate latent class analysis (LCA), with subsequent pairwise comparisons performed using t-tests and an FDR threshold of 5%. All analyses were conducted using GraphPad Prism software, version 9.

3. Results

3.1. Cell-Free Supernatant from Lr6127 Inhibited the Growth of E.coli, C. perfringens and S. typhimurium Isolates

To first assess whether Lr6127 exerts direct antimicrobial effects against clinically relevant canine enteric pathogens, we evaluated the impact of its cell-free supernatant (CFS) on pathogen growth under controlled in vitro conditions. Pathogen growth inhibition was quantified as percentage inhibition normalized to the medium control following 16 h of incubation. No inhibition was observed in the medium control, whereas exposure to Lr6127 CFS resulted in marked suppression of *E.coli, C. perfringens* and *S. typhimurium* growth (Figure 1A).

Across all isolates, average inhibition of *E. coli* growth was 52.0 ± 1.3%, while *C. perfringens* showed an average inhibition of 54.0 ± 2.7%. Growth of *S. typhimurium* was inhibited by 48.6 ± 1.2%. The inhibition by Lr6127 CFS was highly significant for all three pathogen groups relative to the medium control ($p < 0.0001$; Figure 1A).

Dose–response analysis further demonstrated that pathogen growth inhibition increased progressively with increasing volumes of Lr6127 CFS added to the coculture (Figure 1B). For example, *E. coli* growth inhibition increased from 12.8 ± 0.7% at 10 µL CFS to 58.2 ± 1.0% at 40 µL CFS, illustrating a strong concentration-dependent effect. Similar dose-dependent trends were observed for *C. perfringens* and *S. typhimurium*, although inhibition of S. typhimurium remained lower at equivalent CFS volumes. Statistically significant inhibition relative to the medium control was observed at multiple CFS volumes, with significance levels ranging from $p < 0.05$ to $p < 0.0001$ as indicated in the Figure 1B.

3.2. Antimicrobial and Aromatic Amino Acid–Derived Metabolites in Lr6127 CFS and Corresponding Genomic Features

To identify metabolites that may contribute to the growth-inhibitory effects of Lr6127 CFS observed in pathogen inhibition assays (Figure 1), untargeted metabolomic profiling was performed on Lr6127 CFS and the corresponding medium control.

 doi:10.20944/preprints202605.1341.v1

Several antimicrobial-associated metabolites were significantly enriched in Lr6127 CFS compared with the medium control (Figure 2). Indole-3-lactic acid, an indole-derived tryptophan metabolite commonly produced by lactic acid bacteria, was detected at high abundance in Lr6127 CFS, whereas it was not detected in the medium control ($P < 0.001$). Phenylacetic acid, an aromatic organic acid derived from phenylalanine metabolism, was likewise absent from the medium control and present at $3.1 \pm 0.1 \times 10^4$ in Lr6127 CFS ($P < 0.001$).

DL-3-phenyllactic acid, an aromatic lactic acid derivative frequently associated with microbial fermentation, showed marked enrichment in Lr6127 CFS, compared with a low background level in the medium control (559 fold, $P < 0.001$). Similarly, p-hydroxyphenyllactic acid, a hydroxylated aromatic lactic acid commonly linked to microbial metabolism, was significantly elevated in Lr6127 CFS ($P < 0.001$). L-phenylalanine, an essential aromatic amino acid and central precursor in phenyl-derived metabolism, was also present at higher abundance in Lr6127 CFS relative to the medium control ($P < 0.001$).

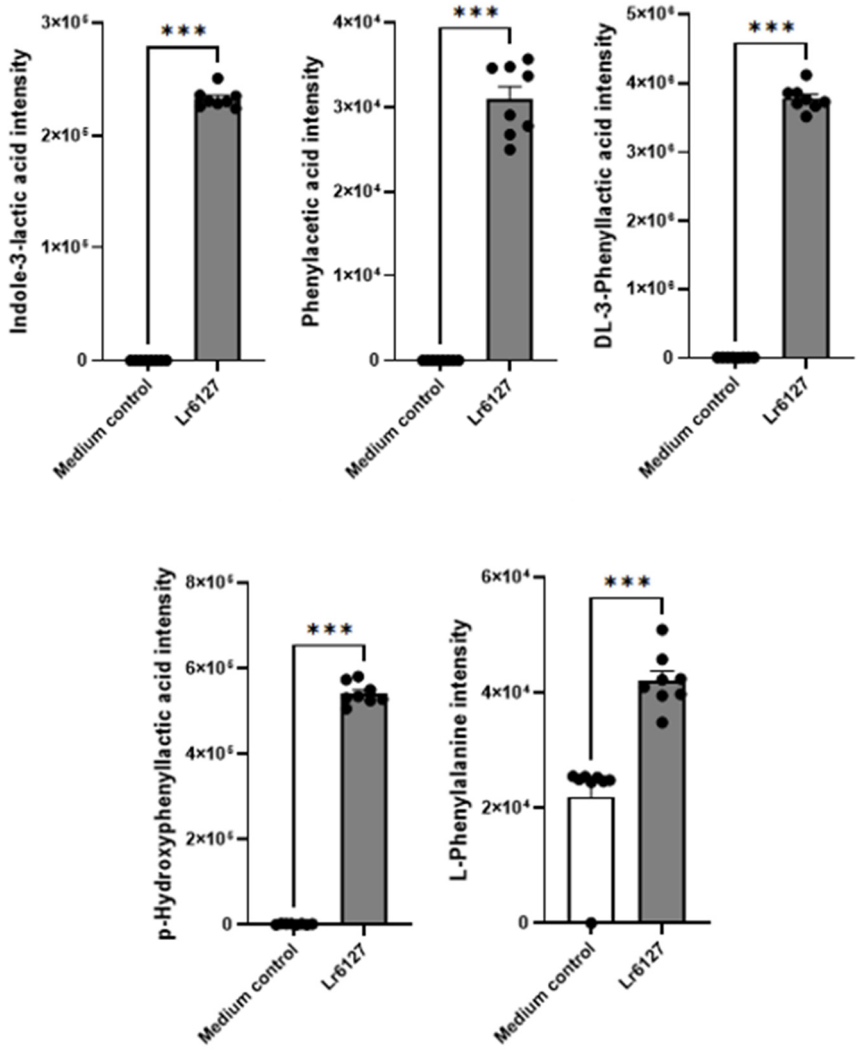

Figure 2. Abundance of antimicrobial-associated metabolites in CFS from Lr6127 determined by untargeted metabolomics. Indole-3-lactic acid, phenylacetic acid, DL-3-phenyllactic acid, p-hydroxyphenyl lactic acid, and L-phenylalanine are shown. Data are presented as means ± standard error (SE) from eight replicates per treatment. Statistical significance was determined by comparison with the medium control. *** $P < 0.001$.

Alongside the enrichment of aromatic amino acid–derived metabolites detected in the Lr6127 cell-free supernatant (CFS), genomic analysis identified adjacent aromatic amino acid

 doi:10.20944/preprints202605.1341.v1

aminotransferase (ArAT) and aromatic lactate dehydrogenase (ALDH) homologs within a single gene cluster in the Lr6127 genome, indicative of the presence in this genome of the classical aromatic amino-acid catabolism pathway, the activity of which is consistent with the elevated abundance of all detected metabolites, except L-phenylalanine

3.3. Lr6127 Colony Forming Units Excluded Pathogen Adhesion to MCA-B1 Cells

Following the identification of antimicrobial-associated metabolites in Lr6127 cell-free supernatant, we next examined whether viable Lr6127 affects pathogen interactions at the epithelial surface. In a preliminary assay, the binding of Lr6127 to MCA-B1 cells was observed following 30 min of co-culture, with an average attachment of 2.0 ± 0.3%. Based on this interaction, adhesion exclusion assays were subsequently performed to determine whether viable Lr6127 could interfere with pathogen attachment to host epithelial cells. MCA-B1 cells were pre-treated with Lr6127 colony-forming units (CFU) prior to pathogen exposure, and pathogen adhesion was quantified as percentage exclusion relative to the control condition, in which MCA-B1 cells were exposed to pathogens in the absence of Lr6127 (Figure 3).

(**A**)

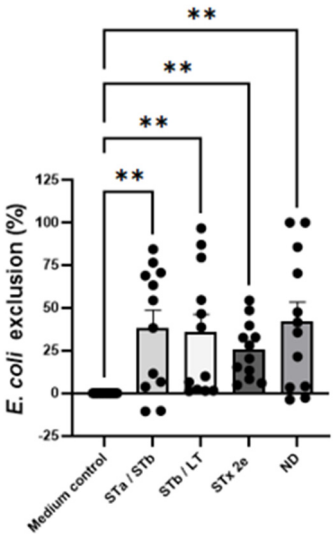

(**B**)

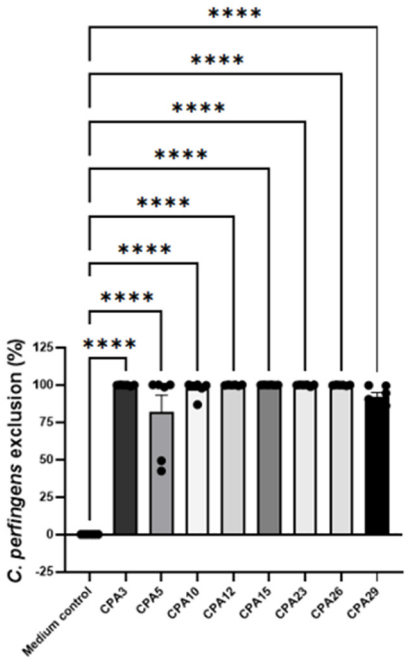

 doi:10.20944/preprints202605.1341.v1

(**C**)

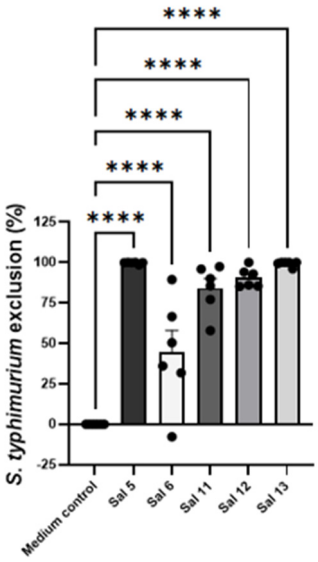

Figure 3. Percentage exclusion of pathogen adhesion to MCA-B1 cells following pre-treatment with Lr6127. (A) Exclusion of *E. coli* isolates representing heat-stable enterotoxin a/b (STa/STb), heat-stable enterotoxin b/heat-labile enterotoxin (STb/LT), Shiga toxin 2e (STx2e), and non-defined (ND) subtypes; (B) Exclusion of individual *C. perfringens* isolates; (C) Exclusion of individual *S. typhimurium* isolates. Data are presented as mean ± standard error (SE) and were obtained from three independent experiments with six technical replicates per isolate. Statistical comparisons were performed relative to the control condition (MCA-B1 cells exposed to pathogens in the absence of Lr6127). ** $P < 0.01$; **** $P < 0.0001$.

Pre-treatment with Lr6127 significantly reduced adhesion of *E. coli* isolates representing multiple toxin subtypes to MCA-B1 cells (Figure 3A). Mean exclusion of STa/STb isolates, expressing heat-stable enterotoxins a and b (STa, STb), was 38.2 ± 10.3%, while STb/LT isolates, expressing heat-stable enterotoxin b and heat-labile enterotoxin (LT), showed a mean exclusion of 35.5 ± 10.6%. Adhesion of STx2e isolates, producing Shiga toxin 2e (STx2e), was reduced by 25.3 ± 4.8%. Non-defined (ND) *E. coli* isolates exhibited the highest exclusion, averaging 42.0 ± 11.3%. All E. coli subtypes displayed significantly reduced adhesion relative to the control condition ($P < 0.01$; Figure 3A).

Lr6127 pre-treatment resulted in pronounced exclusion of *C. perfringens* (A type) adhesion across all tested isolates (Figure 3B). Near-complete exclusion was observed for isolates CPA3, CPA12, CPA15, CPA23, and CPA26, with mean exclusion values ranging from 99.7 ± 0.2% to 100.0 ± 0.0%. CPA10 also exhibited strong exclusion (97.3 ± 2.1%). While exclusion of CPA5 and CPA29 was more variable, mean values remained high at 81.7 ± 11.4% and 91.8 ± 3.1%, respectively. All *C. perfringens* isolates showed highly significant reductions in adhesion compared with the control condition ($P < 0.0001$; Figure 3B).

Similarly, adhesion of *S. typhimurium* isolates to MCA-B1 cells was significantly reduced following Lr6127 pre-treatment (Figure 3C). Near-complete exclusion was observed for isolate Sal 5 (99.8 ± 0.2%) and Sal 13 (99.2 ± 0.6%). Sal 11 and Sal 12 exhibited substantial exclusion, averaging 84.0 ± 6.0% and 90.6 ± 2.5%, respectively. In contrast, Sal 6 displayed greater variability, with a mean exclusion of 44.5 ± 13.5%. Despite this variability, all *S. typhimurium* isolates showed statistically significant reductions in adhesion relative to the control ($P < 0.0001$; Figure 3C).

3.4. Cell-Free Supernatant from Lr6127 Facilitated Wound Healing

Because pathogen adhesion represents an early step in epithelial barrier disruption, we next examined whether Lr6127 cell-free supernatant (CFS) influences subsequent epithelial wound repair. The effect of Lr6127 cell-free supernatant (CFS) on epithelial wound repair was assessed using a

 doi:10.20944/preprints202605.1341.v1

wound healing assay on MCA-B1 cells and wound closure was monitored - over a 10-day culture period. Representative images showed comparable wound areas at day 0, whereas a visibly reduced wound area was observed in CFS-treated monolayers compared with the medium control by day 9 (Figure 4A).

Quantitative analysis of wound closure kinetics was performed using the cumulative area under the curve (AUC) of log-transformed and normalized wound area values using the medium control as center. When summed from days 1 to 9, the cumulative wound area was −0.0 ± 0.6 for the medium control and −1.4 ± 0.6 for Lr6127 CFS-treated cells, indicating significantly enhanced wound closure by day 9. Inclusion of day 10 further strengthened this effect, with summed wound area values of −0.0 ± 0.9 for the control group and −2.8 ± 0.9 following CFS treatment (Figure 4B). Pair-wise statistical comparisons demonstrated that wound area reduction in the Lr6127 CFS-treated group was significant at both day 9 and day 10 relative to the medium control ($P < 0.05$; Figure 4B).

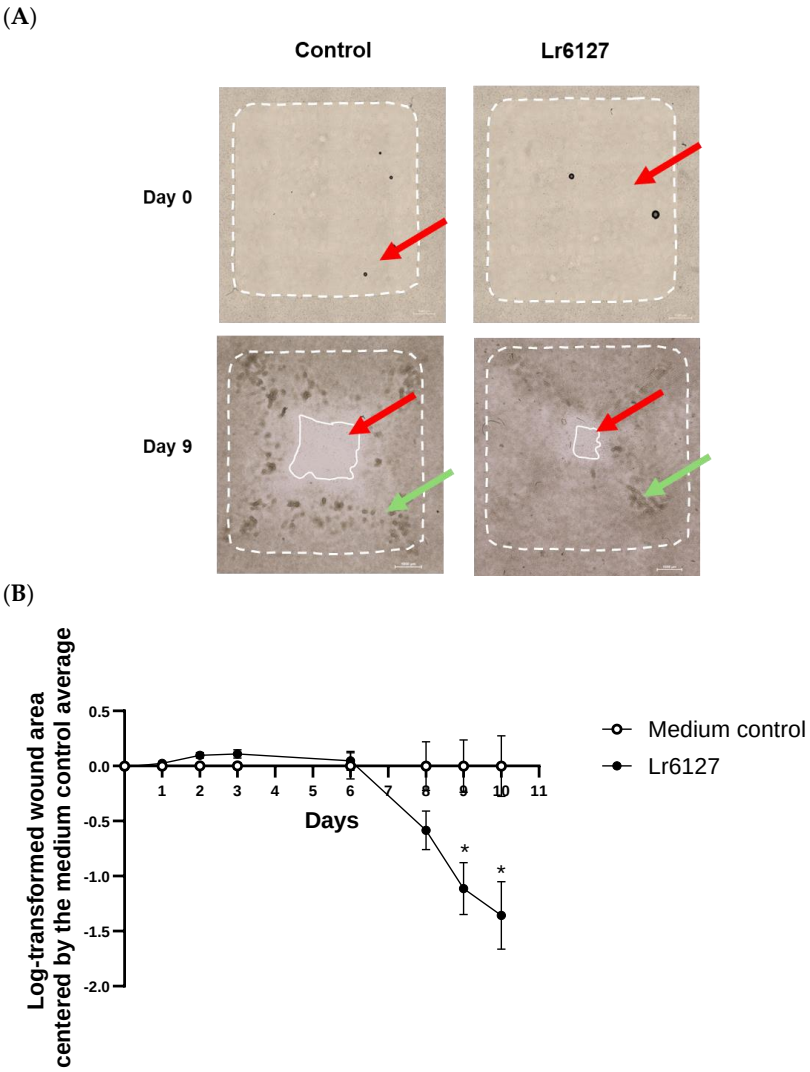

Figure 4. Effect of Lr6127 cell-free supernatant (CFS) on wound healing in MCA-B1 cells. (A) Representative images showing reduced wound area (outlined in red) in Lr6127 CFS-treated MCA-B1 monolayers compared with the MRS medium control on day 9 (dashed square). Green arrows indicate regions of epithelial healing; (B) Wound closure kinetics expressed as the cumulative area under the curve of normalized wound area values. Wound area data was log-transformed and normalized using the mean of the medium control group as center. Values from days 1–10 were summed for each biological replicate and used for comparison between groups. Data represent three independent replicates per treatment. Pair-wise comparisons to the medium control were performed, and statistically significant differences were observed at both day 9 and day 10. $P < 0.05$. .

 doi:10.20944/preprints202605.1341.v1

3.5. Proteomic Identification Wound-Healing Proteins in MCA-B1 Cells Cultured with Lr6127 CFS

Building on the observed enhancement of epithelial wound closure induced by Lr6127 CFS in MCA-B1 cells, we next examined whether this functional response was accompanied by changes in the abundance of proteins known to participate in tissue remodeling, cytoskeletal organization, and cell migration. To this end, the abundance of wound-healing-related proteins was quantified in MCA-B1 cells following exposure to Lr6127 CFS (Figure 5).

Treatment with Lr6127 CFS resulted in a pronounced and significant increase in alpha-2-macroglobulin, a multifunctional protease inhibitor that contributes to extracellular matrix remodeling during tissue repair. Protein abundance increased from 2.3 ± 0.2 in the medium control group to $9.2 \pm 1.9 \times 10^2$ following CFS treatment ($P < 0.05$).

Similarly, the abundance of Ras-related protein Rab-21, which plays a role in vesicular trafficking and integrin-mediated cell migration, was significantly elevated in response to CFS treatment, increasing from $4.0 \pm 0.1 \times 10^3$ in the medium control to $4.7 \pm 0.1 \times 10^3$ ($P < 0.05$). Proteins involved in calcium-dependent regulation of cytoskeletal dynamics were likewise affected, with the EF-hand domain-containing protein showing a moderate but significant increase from $1.7 \pm 0.1 \times 10^5$ to $2.0 \pm 0.1 \times 10^5$ following CFS exposure ($P < 0.05$). In addition, vasodilator-stimulated phosphoprotein, a key mediator of actin filament assembly and directional cell migration, was significantly increased compared with the medium control, rising from $3.5 \pm 0.1 \times 10^4$ to $3.9 \pm 0.2 \times 10^4$ ($P < 0.05$).

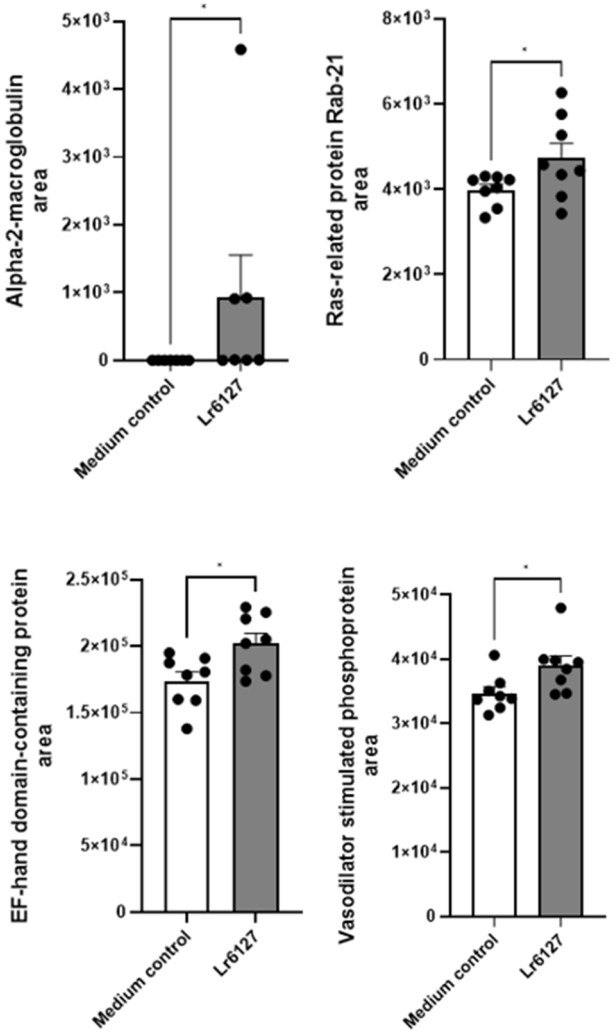

Figure 5. Abundance of wound-healing-related proteins in MCA-B1 cells following exposure to Lr6127 cell-free supernatant (CFS). Protein levels of alpha-2-macroglobulin, Ras-related protein Rab-21, EF-hand

 doi:10.20944/preprints202605.1341.v1

domain-containing protein, and vasodilator-stimulated phosphoprotein were quantified in MCA-B1 cells cultured with Lr6127 CFS or medium control. Data are presented as means with associated standard error (SE) bars. The experiment was performed with eight replicates per treatment group. ns, not significant; $P < 0.05$.

4. Discussion

This study provides in vitro evidence that *Limosilactobacillus reuteri* ATCC PTA 6127 (Lr6127) is associated with effects relevant to epithelial barrier function. Using a canine intestinal epithelial cell model, we show that Lr6127 was associated with reduced pathogen growth and adhesion, and increased wound closure through coordinated changes in wound-healing-associated proteins. Together, these findings are consistent with multiple probiotic-associated effects in vitro [8,9].

Lr6127 cell-free supernatant (CFS) significantly inhibited the growth of *Escherichia coli, Clostridium perfringens*, and *Salmonella typhimurium* in a dose-dependent manner, indicating that antimicrobial activity scales with metabolite exposure rather than reaching a fixed threshold. These pathogens represent distinct modes of epithelial disruption in dogs, including toxin-mediated secretory or cytotoxic damage by *E. coli* [3,4], toxin-driven epithelial injury associated *with C. perfringens* type A [6,7], and epithelial invasion and inflammatory signaling induced by *S. typhimurium* [14]. The consistent inhibition observed across these biologically diverse pathogens is consistent with a broad antimicrobial effect relevant to canine gastrointestinal health.

Untargeted metabolomic profiling identified multiple antimicrobial-associated metabolites enriched in Lr6127 CFS, including indole-3-lactic acid (ILA), DL-3-phenyllactic acid (PLA), p-hydroxyphenyllactic acid (p-HPLA), and phenylacetic acid. ILA, an indole-derived tryptophan metabolite produced by lactic acid bacteria, has been shown to inhibit *E. coli* growth and affect epithelial barrier responses via host signaling pathways [3,15]. PLA and p-HPLA exhibit broad antimicrobial activity against Gram-negative enteropathogens and *Clostridium* species through environmental acidification and membrane perturbation [16,17], while phenylacetic acid has been reported to interfere with bacterial metabolism under gut-relevant conditions [18]. Importantly, no single metabolite detected in Lr6127 CFS is known to fully explain the breadth or magnitude of inhibition observed. Instead, the concurrent presence of metabolites with complementary antimicrobial modes of action, together with the proportional dose–response pattern, suggests that inhibition is mediated by the combined activity of the metabolite pool rather than by a single dominant compound. For example, acid-mediated membrane perturbation by PLA and p-HPLA may plausibly increase bacterial susceptibility to indole-derived metabolites such as ILA, supporting a potential additive or synergistic antimicrobial effect at the biological level [15–17].

To place the observed aromatic amino acid–derived metabolite profile of Lr6127 in a broader biological context, it is useful to consider the metabolic and genomic features associated with aromatic amino acid catabolism in lactic acid bacteria [19]. Conversion of aromatic amino acids into indole- and phenyl-derived metabolites in lactic acid bacteria has been described to proceed through a multistep pathway that is largely inferred from comparative genomics and metabolomics [19,20]. To date, only two enzymes involved in this process have been experimentally characterized in lactic acid bacteria: an aromatic amino acid aminotransferase (ArAT), which catalyzes the initial transamination of aromatic amino acids to their corresponding aromatic pyruvic acids, and an aromatic lactate dehydrogenase (ALDH), which reduces these intermediates to aromatic lactic acids [16,17]. In this context, the identification of adjacent ArAT and ALDH homologs within the Lr6127 genome provides biological context for the enrichment of aromatic amino acid–derived metabolites observed in the cell-free supernatant. Although transcriptional regulation and enzymatic activity were not assessed in the present study, this genomic organization is consistent with previously described metabolic frameworks in lactic acid bacteria and may contribute to the focused aromatic metabolite profile detected for Lr6127 [19].

In addition to these epithelial-intrinsic mechanisms, bacterially derived indole metabolites such as indole-3-lactic acid have been reported to engage aryl hydrocarbon receptor (AhR) signaling and have been associated with epithelial barrier effects in other experimental systems [19,21]. While

 doi:10.20944/preprints202605.1341.v1

AhR-dependent responses were not directly assessed here, the presence of ILA in Lr6127 CFS provides relevant biological context for the barrier-supportive effects observed in this study.

Beyond limiting pathogen growth, Lr6127 provided a second defensive layer by significantly reducing adhesion of multiple *E. coli* toxin subtypes, *C. perfringens* type A isolates, and *S. typhimurium* to canine epithelial cells. Because epithelial attachment is a prerequisite for toxin delivery and invasion, particularly for enterotoxigenic and invasive pathogens, this exclusion effect likely contributes meaningfully to intestinal defense [8,14]. The observation that pathogen exclusion occurred despite relatively modest Lr6127 adhesion is consistent with the possibility that even limited or transient epithelial interactions and competition for binding sites may contribute to impair early pathogen attachment, although the precise mechanisms were not directly examined in the current study. Compared with spore-forming *Bacillus* strains previously evaluated in porcine epithelial models, Lr6127 appears to reduce pathogen adhesion through early interactions at the epithelial interface rather than through extensive or persistent colonization [12].

Importantly, suppression of pathogen pressure was accompanied by enhanced epithelial wound healing, with statistically significant effects emerging only at later time points. This delayed response indicates that Lr6127 CFS may be associated with sustained epithelial remodeling and barrier restoration processes, which are characteristic of mature mucosal repair rather than rapid, transient closure [22,23]. Rather than acting independently, the proteins modulated by Lr6127 CFS can therefore be interpreted as components of a coordinated epithelial repair module. Increased alpha-2-macroglobulin likely stabilizes the extracellular wound microenvironment by limiting excessive protease activity, thereby preserving a provisional matrix scaffold required for effective integrin-dependent migration [24]. Within this stabilized context, the concurrent upregulation of vasodilator-stimulated phosphoprotein (VASP) is consistent with processes involved in epithelial migration, although functional coupling was not directly assessed. [22,23]. Ras-related protein Rab-21 provides a critical link between cytoskeletal remodeling and adhesion dynamics by regulating integrin trafficking, thereby synchronizing cell movement with adhesion turnover and subsequent re-anchoring [25]. The concomitant increase in an EF-hand domain-containing calcium-binding protein further suggests calcium-dependent coordination of these processes, facilitating the transition from active migration to junctional reassembly and barrier stabilization, a sequence that plausibly explains the delayed yet sustained wound-healing response observed [26]. Together with these epithelial-intrinsic mechanisms, prior studies on *L. reuteri* have also highlighted broader host-associated pathways, including oxytocin-linked signaling, that may reinforce tissue repair *in vivo* [27], providing complementary context for the wound-healing effects observed here.

When considered collectively, the combined effects of pathogen growth inhibition, adhesion exclusion, and epithelial repair are consistent with a model in which Lr6127 may be associated with multiple pathogen- and epithelial-related effects. Direct suppression of pathogen proliferation and epithelial colonization reduces luminal and surface-associated pathogen burden, while enhanced wound healing preserves epithelial continuity and limits microbial translocation, a key driver of intestinal inflammation [3]. Rather than acting through a single dominant pathway, Lr6127 integrates antimicrobial metabolite production with host barrier resilience, a layered defense strategy particularly well suited to the dynamic and stress-responsive canine gut environment [1].

This study contributes contextual insight into the associations between Lr6127 and epithelial defense and repair in a canine-relevant cell model, thereby providing a basis for further translational investigation. The use of a two-dimensional canine epithelial system enables controlled examination of host–microbe interactions and probiotic-mediated effects, although it does not fully capture the complexity of the intestinal microenvironment, including mucus layers, commensal microbiota, immune cell contributions, and mechanical forces present in vivo. Pathogen inhibition was assessed under defined in vitro conditions using a representative panel of clinically relevant enteric pathogens, allowing specific associations to be drawn between microbial metabolites and epithelial responses. While the upstream signaling pathways linking Lr6127-derived metabolites to epithelial regulatory networks remain incompletely characterized, the coordinated antimicrobial, adhesion-exclusion, and

 doi:10.20944/preprints202605.1341.v1

wound-healing responses observed in this study indicate biologically relevant probiotic activity. Further investigation using more physiologically complex systems, such as canine intestinal organoids and well-designed in vivo studies, will be necessary to confirm translational relevance, refine dosing strategies, and evaluate long-term safety and efficacy. Integration of multi-omics approaches in such models may further elucidate how microbial metabolites, epithelial signaling pathways, and immune modulation interact to produce the coordinated probiotic effects described here.

5. Conclusions

Limosilactobacillus reuteri ATCC PTA 6127 was associated with pathogen growth inhibition, reduced epithelial adhesion, and enhanced epithelial wound closure in a canine epithelial model. Together, these antimicrobial and epithelial-associated effects support further investigation of Lr6127 as a candidate dog-specific probiotic for intestinal health.

Supplementary Materials: The following supporting information can be downloaded at the website of this paper posted on Preprints.org. Table S1: Identification and genetic characterization of the Enterotoxigenic *Escherichia coli* (ETEC), *Clostridium perfringens* and *Salmonella* isolates used in the assays.

Author Contributions: Conceived and designed the experiment: A.H. and C.S. Performed the experiment: J.W., A.R., A.C.U., K.B.L., A.S., S.Y.B., S.G. W.Z. and C.S. Statistical analysis of data: N. C. and C.S. Wrote and revised the paper: C.S. All authors have read and agreed to the published version of the manuscript.

Funding: This research was funded by Danisco Animal Nutrition & Health (IFF). No specific grant from any funding agency in the public or not-for-profit sectors was received.

Data Availability Statement: The datasets generated in this study are available upon request from

the corresponding author.

Conflicts of Interest: The authors declare that they have no known competing financial interests or

personal relationships that could have appeared to influence the work reported in this paper. All the authors are employees of Danisco Animal Nutrition (IFF).

Abbreviations

The following abbreviations are used in this manuscript:

Abbreviation	Definition
A2M	Alpha-2-macroglobulin
CFS	Cell-free supernatant
CFU	Colony-forming units
EF-hand	EF-hand domain-containing protein
ILA	Indole-3-lactic acid
LT	Heat-labile enterotoxin
MYL6B	Myosin light chain 6B
OD	Optical density
PLA	Phenyllactic acid
p-HPLA	p-Hydroxyphenyllactic acid
Rab21	Ras-related protein Rab-21
SE	Standard error
STa	Heat-stable enterotoxin a

 doi:10.20944/preprints202605.1341.v1

STb	Heat-stable enterotoxin b
STx2e	Shiga toxin 2e
VASP	Vasodilator-stimulated phosphoprotein

References

1. Marks, S.L.; Kather, E.J. Bacterial-associated diarrhea in the dog: A critical appraisal. Veterinary Clinics of North America: Small Animal Practice 2003, 33, 1029–1060.
2. Leonard, E.K.; Pearl, D.L.; Finley, R.L.; Janecko, N.; Reid-Smith, R.J.; Weese, J.S. Evaluation of pet-related management factors and the risk of Salmonella shedding in dogs. Zoonoses Public Health 2011, 58, 140–146.
3. Nagao, I.; Kawasaki, M.; Goyama, T.; Kim, H.J.; Call, D.R.; Ambrosini, Y.M. Enterohemorrhagic Escherichia coli disrupts intestinal barrier integrity in translational canine stem cell-derived monolayers. Microbiology Spectrum 2024, 12, e00961-24.
4. De Luca, G.; Costantini, G.; Borrelli, L.; Izzo, P.; Riccone, N.; Del Piano, F.; Valvini, O.; Gallo, A.; Auriemma, C.; Alfano, F.; et al. Toxin-producing Escherichia coli: A long-term retrospective study in dogs and cats between 2017 and 2023. Frontiers in Veterinary Science 2025, 12, 1557445.
5. Wang, H.; Zhong, Z.; Luo, Y.; Cox, E.; Devriendt, B. Heat-stable enterotoxins of enterotoxigenic Escherichia coli and their impact on host immunity. Toxins 2019, 11, 24.
6. Park, J.; Cheon, D.; Oh, Y.-I. Prevalence and toxin gene profiles of Clostridium perfringens in diarrheic dogs and cats: A retrospective analysis. Journal of Veterinary Science 2025, 26, e52.
7. Gohari, I.M.; Parreira, V.R.; Nowell, V.J.; Nicholson, V.M.; Oliphant, K.; Prescott, J.F. A novel pore-forming toxin in type A Clostridium perfringens is associated with fatal canine hemorrhagic gastroenteritis. PLoS ONE 2015, 10, e0122684.
8. Bermudez-Brito, M.; Plaza-Díaz, J.; Muñoz-Quezada, S.; Gómez-Llorente, C.; Gil, A. Probiotic mechanisms of action. Annals of Nutrition and Metabolism 2012, 61, 160–174.
9. Entezami, A.; Zarrini, G. The science behind probiotics: Mechanisms and therapeutic potential. Probiotics and Antimicrobial Proteins 2025, 17, 10820.
10. Zhang, Y.; Zhao, M.; Li, Y.; Liang, S.; Li, X.; Wu, Y.; Li, G. Potential probiotic properties and complete genome analysis of Limosilactobacillus reuteri from dogs. Microorganisms 2024, 12, 1811.
11. Wick, R.R.; Howden, B.P.; Stinear, T.P. Autocycler: Long-read consensus assembly for bacterial genomes. Bioinformatics 2025, 41, btaf474.
12. Rasmussen, P.B.; Walker, J.; Stubbs, S.R.; Udrea, A.C.; Shen, C. Evaluation of probiotic Bacillus velezensis for the control of pathogens that cause post-weaning diarrhea in piglets—Results from in vitro testing and an in vivo model using Caenorhabditis elegans. Microorganisms 2025, 13, 1247.
13. Kadekar, D.; Udrea, A.C.; Bak, S.Y.; Christensen, N.; Gibbs, K.; Shen, C.; Bernardeau, M. Cell-Free Culture Supernatant of Lactobacillus acidophilus AG01 and Bifidobacterium animalis subsp. lactis AG02 Reduces the Pathogenicity of NetB-Positive Clostridium perfringens in a Chicken Intestinal Epithelial Cell Line. Microorganisms 2024, 12, 839.
14. Marks, S.L.; Rankin, S.C.; Byrne, B.A.; Weese, J.S. Enteropathogenic bacteria in dogs and cats: Diagnosis, epidemiology, treatment, and control. J. Vet. Intern. Med. 2011, 25, 1195–1208.
15. Zelante, T.; Iannitti, R.G.; Cunha, C.; De Luca, A.; Giovannini, G.; Pieraccini, G.; Zecchi, R.; D'Angelo, C.; Massi-Benedetti, C.; Fallarino, F.; et al. Tryptophan catabolites from microbiota engage the aryl hydrocarbon receptor and balance mucosal reactivity via interleukin-22. Immunity 2013, 39, 372–385.
16. Mu, W.; Chen, C.; Li, X.; Zhang, T.; Jiang, B. Phenyllactic acid produced by lactic acid bacteria: Structure, antimicrobial activity, and biosynthesis pathway. Biotechnol. Adv. 2012, 30, 33–41.
17. Li, X.; Mu, W.; Jiang, B.; Zhang, T. Antimicrobial activity and mechanism of action of phenyllactic acid against foodborne pathogens. Food Control 2020, 110, 106983.
18. Smith, E.A.; Macfarlane, G.T. Formation of phenylacetic acid and phenylpropionic acid by human gut bacteria. J. Appl. Microbiol. 2015, 118, 1261–1271.
19. Landete, J.M. Aromatic amino acid metabolism by lactic acid bacteria. Food Microbiol. 2012, 31, 221–227.

 doi:10.20944/preprints202605.1341.v1

20. Su, X.; Gao, Y.; Yang, R. Gut microbiota-derived tryptophan metabolites maintain gut and systemic homeostasis. Cells 2022, 11, 2296
21. Zhao, C.; Hu, X.; Bao, L.; Wu, K.; Feng, L.; Qiu, M.; Hao, H.; Fu, Y.; Zhang, N. Aryl hydrocarbon receptor activation by Lactobacillus reuteri tryptophan metabolism alleviates Escherichia coli–induced mastitis in mice. PLoS Pathogens 2021, 17, e1009774.
22. Vicente-Manzanares, M.; Ma, X.; Adelstein, R.S.; Horwitz, A.R. Non-muscle myosin II takes centre stage in cell adhesion and migration. Nat. Rev. Mol. Cell Biol. 2009, 10, 778–790.
23. Krause, M.; Dent, E.W.; Bear, J.E.; Loureiro, J.J.; Gertler, F.B. Ena/VASP proteins: Regulators of the actin cytoskeleton and cell migration. Annu. Rev. Cell Dev. Biol. 2003, 19, 541–564.
24. Laurell, C.B.; Eriksson, S. The electrophoretic α1-globulin pattern of serum in α1-antitrypsin deficiency. Scand. J. Clin. Lab. Investig. 2013, 15, 132–140.
25. Pellinen, T.; Arjonen, A.; Vuoriluoto, K.; Kallio, K.; Fransen, J.A.; Ivaska, J. Small GTPase Rab21 regulates cell adhesion and controls endosomal traffic of β1-integrins. J. Cell Biol. 2006, 173, 767–780.
26. Berridge, M.J.; Bootman, M.D.; Roderick, H.L. Calcium signalling: Dynamics, homeostasis and remodelling. Nat. Rev. Mol. Cell Biol. 2003, 4, 517–529.
27. Poutahidis, T.; Kearney, S.M.; Levkovich, T.; Qi, P.; Varian, B.J.; Lakritz, J.R.; Ibrahim, Y.M.; Chatzigiagkos, A.; Alm, E.J.; Erdman, S.E. Microbial symbionts accelerate wound healing via the neuropeptide hormone oxytocin. PLoS ONE 2013, 8, e78898.